V International Conference on Computational Methods in Marine Engineering
MARINE 2013
B. Brinkmann and P. Wriggers (Eds)

DEFORMATION BEHAVIOUR OF REINFORCED CONCRETE SHELLS FOR OFFSHORE STRCTURES

MARINE 2013

Waldemar Krakowski, Martin Empelmann, Lars Eckfeldt

iBMB – Concrete Construction Department
Technische Universität Braunschweig
Beethovenstraße 52, 38106 Braunschweig, Germany
e-mail: massivbau@ibmb.tu-bs.de, www.ibmb.tu-braunschweig.de

Key words: GBS, reinforced concrete, shell structures, testing, material modelling

1 INTRODUCTION

Gravity base structures (GBS) are shell structures made of reinforced concrete (RC). After past few years with little development activity, interest in robust structures for the arctic environment, as for liquefied natural gas terminals and for special floating barges is growing again (Figure 1) [3]. For the design of GBS extensive knowledge about the material and deformation behaviour is needed.

Figure 1: Gravity base structure “Sakhalin II” in the arctic region (source: *http://gazprom-sh.nl*)

Modelling of the nonlinear deformation behaviour and the cracking process has been examined for reinforced concrete structures as plates, panels and shells in detail. However, the object of investigation was limited to elements with reinforcement parallel to the tension direction. For GBS loads from waves, wind or filling operations vary [8], [14]. The principal stress and strain directions therefore may change. That is why reinforcement in tension will not be stressed ideally, but in a certain skewed angle. Experimental data shows for those cases larger crack widths and deformations as in cases of tension stresses parallel to the

reinforcement [2], [11], [16].

Based on own tests and those from literature a new approach for predicting the deformation behaviour of reinforced concrete structures with arbitrary reinforcement orientation has been formulated.

2 GENERAL CONSIDERATIONS

The deformation behaviour of RC structures in compression is dominated by concrete. In case of tension, cracking of concrete occurs at a very low stress level. Within cracks the steel transfers the whole tension force. Beyond cracks the tension force is transmitted via bond into the concrete again. Therefore, the behaviour in tension as well for steel as for concrete has to be considered adequate in order to achieve a realistic material modelling. The deformation behaviour in compression and tension may be idealized as strut and tie model. This allows a separate consideration in tension and compression. A typical simple application for a beam in bending is shown in Figure 2.

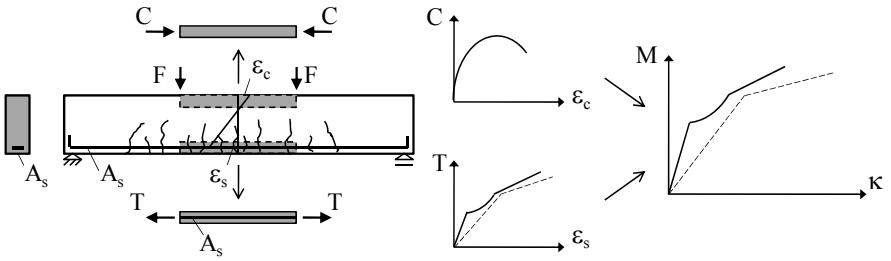

Figure 2: Strut and tie modelling for a beam

The same principles of strut and tie modelling as for beams are applicable to shell structures. However, modelling of shell structures is more complex due to the changing path of tensile stress but fixed position of rebars. Therefore, extended calculation methods have been established, documented in reference [2] and [15]. They allow a very accurate determination of the real load-deformation behaviour for concrete shell structures with arbitrary reinforcement direction. However, these methods include iterative calculation algorithms. The complex algorithms do not allow fast nonlinear calculations in extensive structures modelled by the finite element method (FEM). Therefore, a new approach in closed form is needed, which allows a highly accurate but non-iterative material modelling.

3 FULL SCALE TESTS ON PANELS

3.1 Testing program

Due to the lack of test data from panels under biaxial tension, a new full scale testing facility for concrete members with arbitrary reinforcement orientation has been developed (Figure 3) [7]. One of the requirements to this testing facility has been the free elongation in each loading directions without any restraint due to transverse cracking. Therefore single steel plates have been bolted to the specimen with prestress about 400 Nm (Figure 4). The steel plates have been connected to a cantilever via 50 mm round bars. The round bars have been greased and were enabled to glide on a high strength steel interlayer, which has been placed

between the round bar and the cantilever. Hence, every round bar was able to transfer in-plane forces in the loading direction, but no in-plane force in the transverse direction. In order to avoid bending forces from unwanted eccentricity, a ball nut has been placed on each end of the cantilever. The horizontal and the vertical bearings have been fixed to the floor via prestressed bars for the reason to limiting deformations of the test setup.

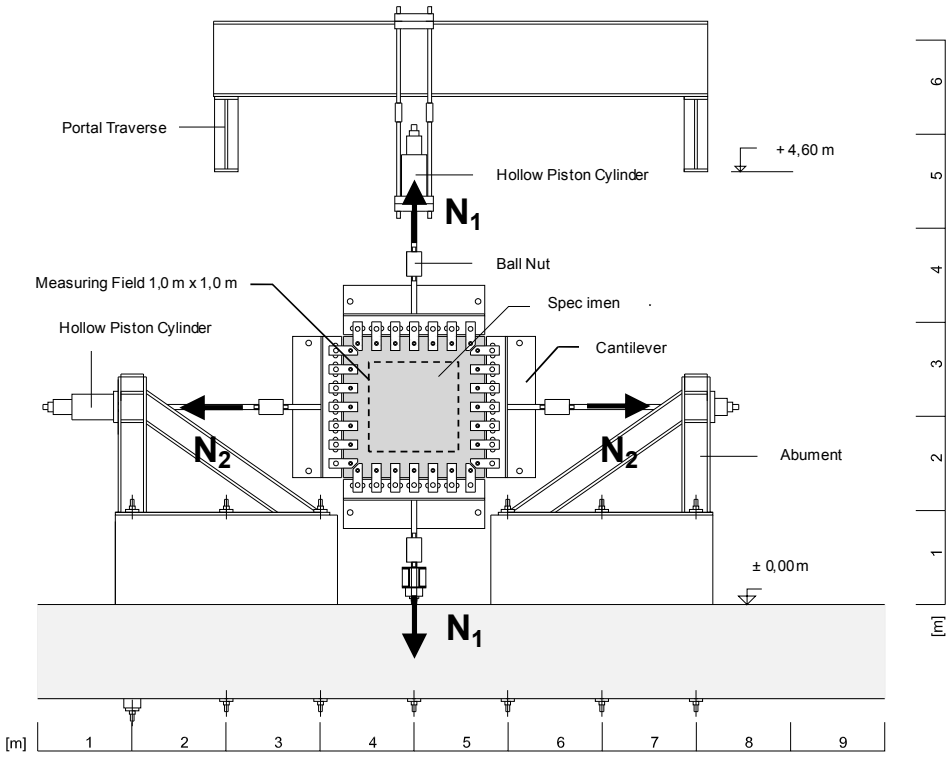

Figure 3: Test setup

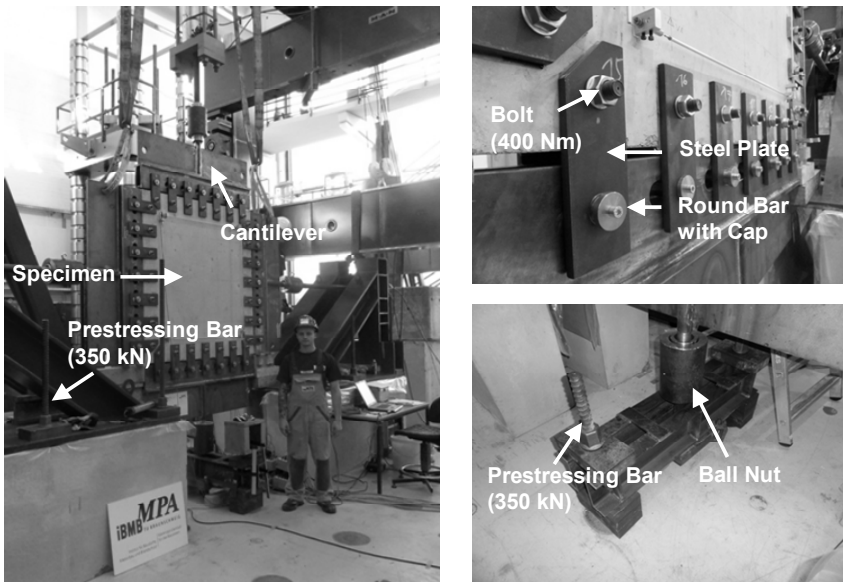

Figure 4: Details of test setup

The specification of every specimen are summarised in Table 1. The bar diameter have been chosen to be 10 mm, except specimen Z3 where bar diameter of 8 mm in the x-direction has been applied ($\lambda = A_{s,x}/A_{s,y} = 0{,}6$). The bar spacing s_x and s_y was constant for all specimen.

Table 1: Specimen specifications

	Θ [°]	$d_{s,x}$ [mm]	$d_{s,y}$ [mm]	s_x [mm]	s_y [mm]	λ [-]	k [-]	$f_{ct,sp}$ [N/mm²]	$f_{c,cyl}$ [N/mm²]
Z1	0	10	10	100	100	1,0	1,0	2,9	31,0
Z2	45	10	10	100	100	1,0	0,0	2,3	25,2
Z3	45	8	10	100	100	0,6	0,5	2,7	30,4
Z4	22,5	10	10	100	100	1,0	0,0	2,9	37,8
Z5	22,5	10	10	100	100	1,0	0,7	3,4	38,8
Z6	22,5	10	10	100	100	1,0	0,5	3,0	30,8

To ensure a certain loading level, the reinforcement was anchored with loops and hooks around a steel bush as shown in Figure 5. The steel bush has been set in position before casting for a later bolting. Each reinforcement direction consisted of one layer, which has been placed at the centre of the specimen. The ribbed reinforcing steel consisted of B500 S with a yield strength $f_{yk} = 500$ N/mm². The main influencing parameters have been chosen to be the reinforcement orientation related to the tension direction with $\Theta = 0°$, 22,5°, 45°, and loading ratio $k = N_2/N_1$.

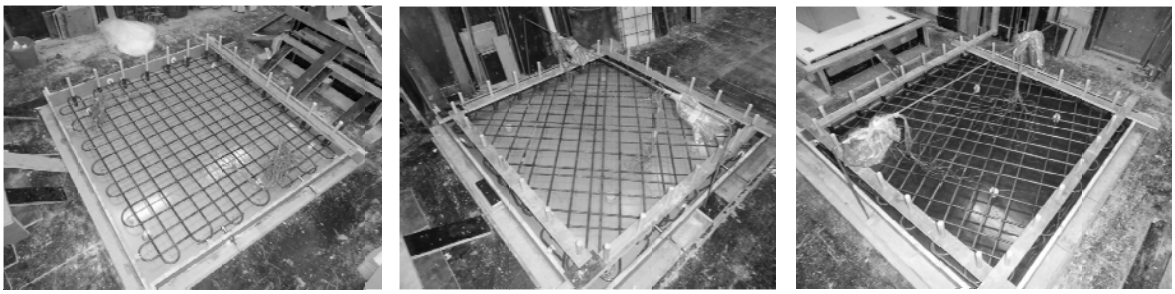

(a) (b) (c)

Figure 5: Formwork and reinforcement: (a) Specimen Z1, (b) specimen Z2 and (c) specimen Z4

The measuring program consisted of longitudinal displacement transducers (LDT) in the loading directions at both sides of the specimen and LDT which have been applied diagonal at one side. Steel strains have been measured via strain gauges, which were glued to the reinforcement before casting. Crack widths have been measured by a special digital camera system with high resolution. Crack formation and crack spacing have been documented too.

3.2 Test results

For increasing loading ratio $k = N_2/N_1$ a decreasing concrete tensile strength σ_{1cr} has been established from the conducted research program, as shown in Figure 6. Herein the concrete tensile strength from specimen has been related to material testing strength (5%-quantile), which shows good accordance for k = 0. The difference between Z2 with k = 0 and Z1 with k = 1 is about 25%. This outcome is confirmed by reference [2].

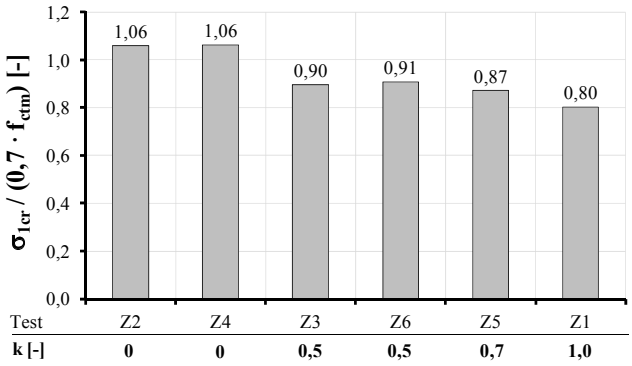

Figure 6: Concrete tensile strength from tests related to the material testing depending on k

It has to be stated, for $k \leq 0,7$ cracking occurred almost perpendicular to N_1 only [7]. For in-plane hydrostatic loading with $k = 1$ the crack pattern of specimen Z1 showed hardly any kind of orientation. Cracking for Z1 was neither oriented on rebars nor on loading directions, whereas for the rest of the series the crack pattern was mostly oriented at the loading direction (Figure 7). Closing of existing cracks and forming of new cracks with severe different orientation has not been noticed during loading for k = const. In reference [9], [11] the crack orientation related to the loading direction has been examined for test series on plates and panels under uniaxial tension. Within the elastic steel strains the crack orientation can be assumed to be perpendicular to the tension direction in uniaxial as well as in biaxial tension with $k \leq 0,7$ (Figure 7). For $k > 0,7$ there is no significant cracking direction. However, for hydrostatic in-plane loading the measured stiffness was the same as in uniaxial tension parallel to reinforcement with σ_0.

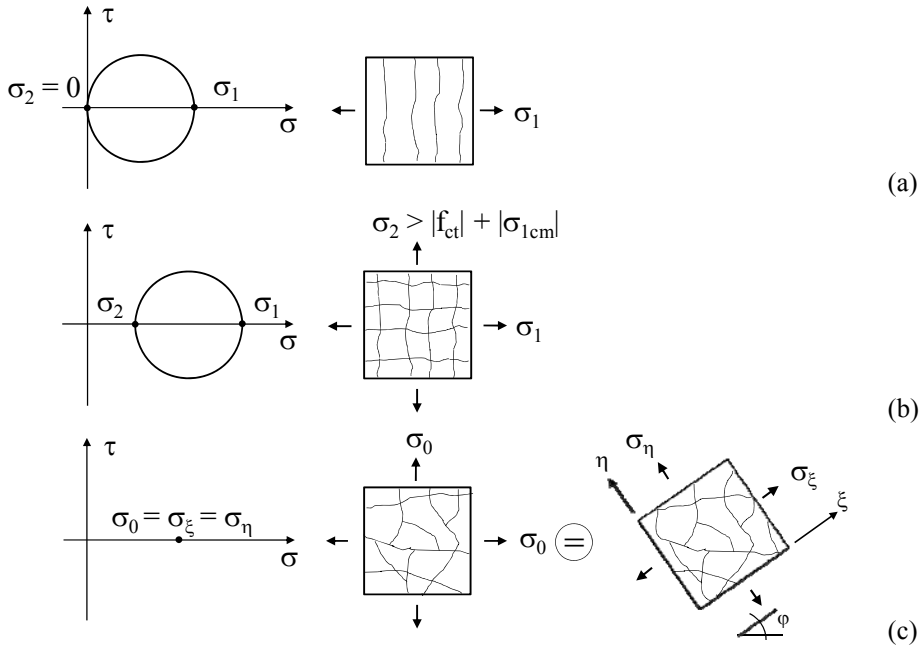

Figure 7: Mohrs cycle: (a) uniaxial tension and crack pattern, (b) biaxial tension and crack pattern, (c) hydrostatic loading and crack pattern

4 MODELLING THE MATERIAL BEHAVIOUR FOR RC STUCTURES

4.1 Concrete in compression

The nonlinear stress-strain relationship of concrete in compression may be expressed trough

$$\frac{\sigma_c}{f_c} = \left(\frac{k \cdot \eta - \eta^2}{1 + (k-2) \cdot \eta} \right) \tag{1}$$

according to EC2 [5] or MC 2010 [3]. When calculation of concrete strains ε_c in the descending brand with Eq. (1) is not needed, the parabola formulation according to EC2 [5] can be rearranged with

$$\frac{\sigma_c}{f_c} = -\left(1 - \left(1 - \frac{\varepsilon_c}{\varepsilon_{c1}}\right)^2\right) \tag{2}$$

and gives comparative results for normal strength concrete in the ascending branch as shown in Figure 8.

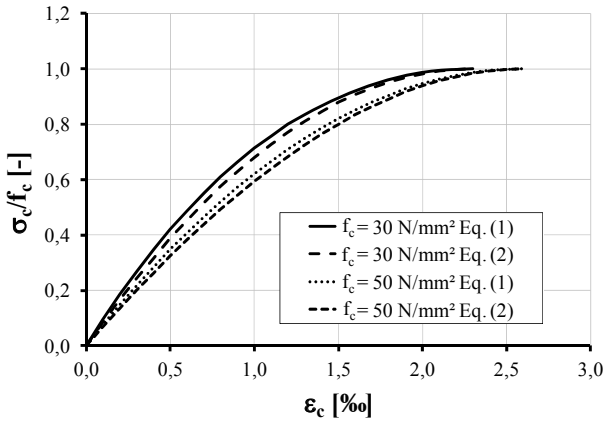

Figure 8: Comparing different formulations for concrete in compression

4.2 Reinforcement steel

Reinforcement steel in compression as well as in tension is characterised trough a constant modulus of elasticity with E_s = 200.000 N/mm². After yielding strain hardening is possible. Strain hardening makes up to 10 % of the yielding stress according to the German provisions for steel class B500 [5]. For sake of simplicity strain hardening can be neglected.

4.3 Reinforced concrete in shear

Shear stress capacity of cracked concrete is limited to a certain value. The mathematical formulation for shear capacity, as proposed in MC 2010 [3], needs an iterative procedure and is applicable to local friction, known as aggregate interlock, only. In reference [11] a formulation for shear capacity of cracked concrete has been established, which can be expressed with

$$\tau_{c,max} = \left(\frac{\rho_x}{0{,}006}\right)^{0,4} \cdot C \cdot \sqrt{f_{c,cyl}}. \tag{3}$$

Herein is

$\tau_{c,max}$ shear capacity of the crack surface,

ρ_x reinforcement ratio in x-direction with $\rho_x = \frac{A_{s,x}}{A_c}$,
the reinforcement cross section $A_{s,x,}$ the concrete cross section A_c,

C factor with $C = \left(\cos^2(\Theta + 15°) + \frac{1}{\lambda} \cdot \sin^2(\Theta)\right)$, $\lambda = \frac{A_{s,x}}{A_{s,y}}$,

$f_{c,cyl}$ concrete cylinder strength in N/mm².

The above mentioned formulation is applicable to uniaxial tension with one way and orthogonal two way reinforcement. It has been verified against test results from reference [12] and [17] (Figure 9) and shows good agreement with experimental values.

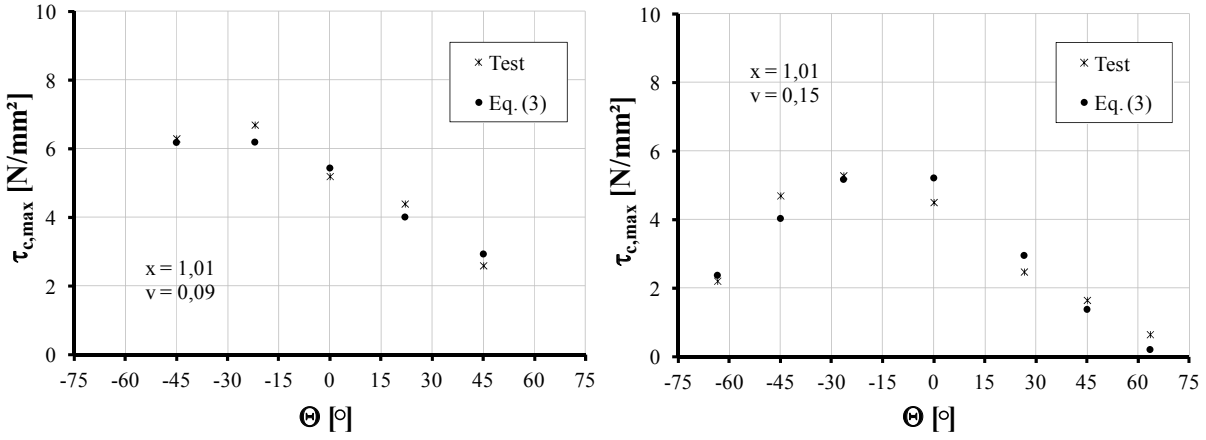

Figure 9: Comparison between test results and Eq. (3) for (a) specimen from [17] and (b) specimen from [12]

5 MODELLING THE DEFORMATION BEHAVIOUR FOR RC STRUCTURES

5.1 Mathematical formulation for pure tension

As mentioned in [2], [9], [16] the orientation of yield lines may deviate from crack orientation in the elastic state of steel strains. Aoyagi [1] compared different calculation methods with fixed and rotating crack angles. He stated for the ultimate loading capacity the crack orientation is not relevant, as all applied methods lead to very similar results. In the following for plastic steel strains the same crack angle as for the elastic strains will be assumed. According to Vecchio & Collins [15], for practical use the relatively small deviation between principal strain direction and principal stress direction will be neglected.

Following failure modes are relevant for shell elements:

- Failure of reinforcement of one or both directions, when ε_{su} is exceeded.
- Failure of concrete, when ε_c exceeds $\varepsilon_{c1.}$

For in-plane loading as for panels, the following failure mode has to be considered too:

- Failure of crack plane when the maximum shear capacity is reached with $|\tau_{c,xy}| = \tau_{c,max}$.

The steel stress may be calculated as proposed in reference [10] with:

$$\sigma_{1s,x} = \frac{\sigma_1 \cdot \cos^2\Theta \cdot A_c}{\left(A_{s,x} \cdot \cos^4\Theta + A_{s,y} \cdot \sin^4\Theta\right)} \leq f_{yk}$$
$$\sigma_{1s,y} = \frac{\sigma_1 \cdot \sin^2\Theta \cdot A_c}{\left(A_{s,x} \cdot \cos^4\Theta + A_{s,y} \cdot \sin^4\Theta\right)} \leq f_{yk} \quad (4)$$

From equilibrium in the crack plane the shear stress follows with:

$$\tau_{1c,xy} = \frac{\left(\sigma_{1s,x} \cdot A_{s,x} - \sigma_{1s,y} \cdot A_{s,y}\right)}{A_c} \cdot \sin\Theta \cdot \cos\Theta \leq \tau_{c,max} \quad (5)$$

On basis of own tests (Figure 6) and tests from reference [2] it has to be stated, the tensile strength of concrete depends not only on the material parameter f_{ct}, but on the interaction of the principal tension stress too. This interaction from biaxial tension can be determined via reduction factor k_t for first cracking with the following expression:

$$k_t = 1 - 0{,}30 \cdot \frac{\sigma_2}{\sigma_1} \leq 1{,}0 \quad (6)$$

According to Figure 2 the tension zone may by expressed on behalf of a modified steel stress-strain-relationship, which has been applied in principal tensile direction (Figure 10).

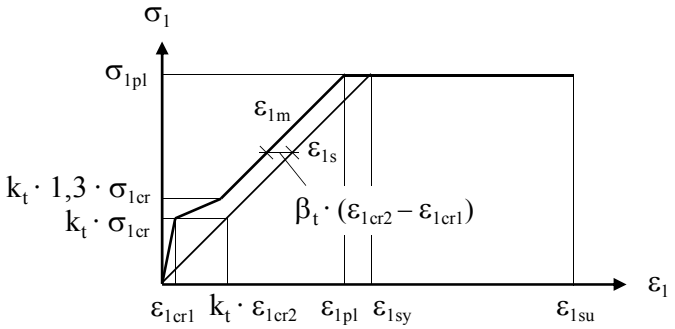

Figure 10: Modified tensile stress-strain-relationship in principal direction

For uncracked concrete ($0 < \varepsilon_{1m} \leq k_t \cdot \varepsilon_{cr1}$) the following formulation of the average strain ε_{1m} has to be applied in the first principal tensile direction:

$$\varepsilon_{1m} = \varepsilon_{1c} \quad (7)$$

For the phase of initial cracking ($k_t \cdot \varepsilon_{1cr1} < \varepsilon_{1m} < k_t \cdot 1{,}3 \cdot \varepsilon_{1cr1}$) the average strain is:

$$\varepsilon_{1m} = \varepsilon_{1s} - \frac{\beta_t \cdot (\sigma_1 - k_t \cdot \sigma_{1cr}) + k_t \cdot (k_t \cdot 1{,}3 \cdot \sigma_{1cr} - \sigma_1)}{k_t \cdot 0{,}3 \cdot \sigma_{1cr}} \cdot (\varepsilon_{1cr2} - \varepsilon_{1cr1}) \quad (8)$$

The average strain within the stabilized cracking stage ($k_t \cdot 1{,}3 \cdot \varepsilon_{1cr1} < \varepsilon_{1m} < \varepsilon_{1pl}$) may be expressed trough:

$$\varepsilon_{1m} = \varepsilon_{1s} - \beta_t \cdot (\varepsilon_{1cr2} - \varepsilon_{1cr1}) \quad (9)$$

Herein is

σ_1 first principal tensile stress,

ε_{1m} first average tensile strain,

ε_{1c} concrete strain before cracking in the first principal tensile direction,

ε_{1cr1} principal tensile strain for uncracked concrete when tensile strength of concrete is reached with $\varepsilon_{1cr1} = \frac{f_{ctm}}{E_c}$,

σ_{1cr} cracking stress $\sigma_{1cr} = f_{ctm} \cdot (1 + \alpha_e \cdot \text{eff}\rho_1^*)$,

ε_{1cr2} principal tensile strain in the crack plane when concrete tensile strength is reached with $\varepsilon_{1cr2} = \frac{f_{ctm} \cdot (1+\alpha_e \cdot \text{eff}\rho_1^*)}{E_s \cdot \text{eff}\rho_1^*}$,

ε_{1s} principal tensile strain in the crack plane with $\varepsilon_{1s} = \frac{\sigma_1 - \sigma_{2cm}}{E_s \cdot \text{eff}\rho_1^*} \geq 0$,

σ_{2cm} average concrete compression stress with $\sigma_{2cm} = \beta_t \cdot \sigma_2 \cdot \frac{\Theta}{45^\circ}$ for $\sigma_2 \geq k_t \cdot 1{,}3 \cdot \sigma_{2cr}$, else $\sigma_{2cm} = 0$,

ε_{1pl} maximum principal tensile strain in the crack plane when yielding is reached with $\varepsilon_{1pl} = \frac{f_{yk} \cdot A_c}{E_s \cdot (A_{s,x} \cdot \cos^4\Theta + A_{s,y} \cdot \sin^4\Theta)}$ and $A_c = h \cdot b$,

$\text{eff}\rho_1^*$ effective reinforcement ratio with $\text{eff}\rho_1^* = \frac{A_{s,x} \cdot \cos^4\Theta + A_{s,y} \cdot \sin^4\Theta}{A_{c,eff}}$,

β_t coefficient for short term loading ($\beta_t = 0{,}4$) and long term loading ($\beta_t = 0{,}25$),

k_t coefficient for interaction between σ_1 and σ_2 according to Eq (6).

In most cases the second principal tensile direction will remain either uncracked or under compression stress. For the special case of additional cracking in the second principal direction, it is referred to reference [11].

5.2 Mathematical formulation for combined in-plane loading

On basis of the material behaviour as defined in the previous sections and the fundamental mechanical principles for in-plane loading, a new approach for combined loads will be derived. The following expressions are based on the definitions as shown in Figure 11.

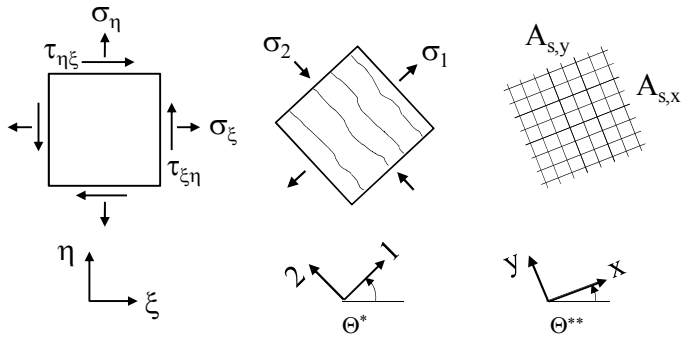

Figure 11: Definition of coordinate system: (a) general loading direction, (b) direction of principal stresses with crack pattern and (c) direction of reinforcement

Between the general loading and the principal stress directions the following geometric definition holds:

$$\tan 2\Theta^* = \frac{2 \cdot \tau_{\xi\eta}}{\sigma_\xi - \sigma_\eta} \tag{10}$$

Herein is

Θ^* angle between the $\xi\eta$-coordinates and principal stress coordinates,
$\tau_{\xi\eta}$, σ_ξ, σ_η loading stress.

On basis of Mohrs cycle the principal stresses are:

$$\sigma_{1,2} = \frac{(\sigma_\xi + \sigma_\eta)}{2} \pm \sqrt{\left(\frac{\sigma_\xi - \sigma_\eta}{2}\right)^2 + {\tau_{\xi\eta}}^2} \tag{11}$$

The reinforcement stresses are determined as defined in Eq (4). The average strain ε_{1m} is calculated as proposed in section 5.1. As stated by Veccio & Collins [15] compressive strength of concrete decreases as the average strain ε_{1m} in the first principal direction increases. Therefore, a modification of the expression for Eq. (2) according to [15] has been adopted. Rearanging Eq. (2) and consideration of a decreasing compressive strength can be expressed in closed form with:

$$\varepsilon_{2m} = \varepsilon_{c1} \cdot \left(1 - \sqrt{\frac{\sigma_2}{f_c^*} + 1}\right) \leq \varepsilon_{c1} \tag{12}$$

Herein is

ε_{2m} second principal compressive strain,
ε_{c1} maximum compressive concrete strain
(ε_{c1} for normal strength concrete with 2,0 ‰),
f_c^* reduced compressive strength due to transversal strain.

For the reduced compressive concrete strength the following expression holds:

$$\frac{f_c}{f_c^*} = \frac{1}{0{,}8 + 0{,}34 \cdot \frac{\varepsilon_{1m}}{\varepsilon_{c1}}} \tag{13}$$

Herein is

f_c uniaxial compressive concrete strength,
ε_{1m} average tensile strain ε_{1m}.

Deformations of the $\xi\eta$-system are calculated with back transformation from the principal strains as following:

$$\begin{aligned} \varepsilon_{\xi m} &= \varepsilon_{1m} \cdot \cos^2\Theta^* + \varepsilon_{2m} \cdot \sin^2\Theta^* \\ \varepsilon_{\eta m} &= \varepsilon_{1m} \cdot \sin^2\Theta^* + \varepsilon_{2m} \cdot \cos^2\Theta^* \\ \gamma_{\xi\eta m} &= 2 \cdot (\varepsilon_{1m} - \varepsilon_{2m}) \cdot \sin\Theta^* \cdot \cos\Theta^* \end{aligned} \tag{14}$$

6 MODEL VERIFICATION

Panel tests performed by Peter [13] show a load-deformation behaviour depending on the reinforcement orientation Θ. In Figure 12 for S 2r 0 with Θ = 0° as well as for S 2r 40 with Θ = 40° good accordance between calculated values and values from tests has been achieved. Influence of skew reinforcement has been considered accurately within calculations by the new approach.

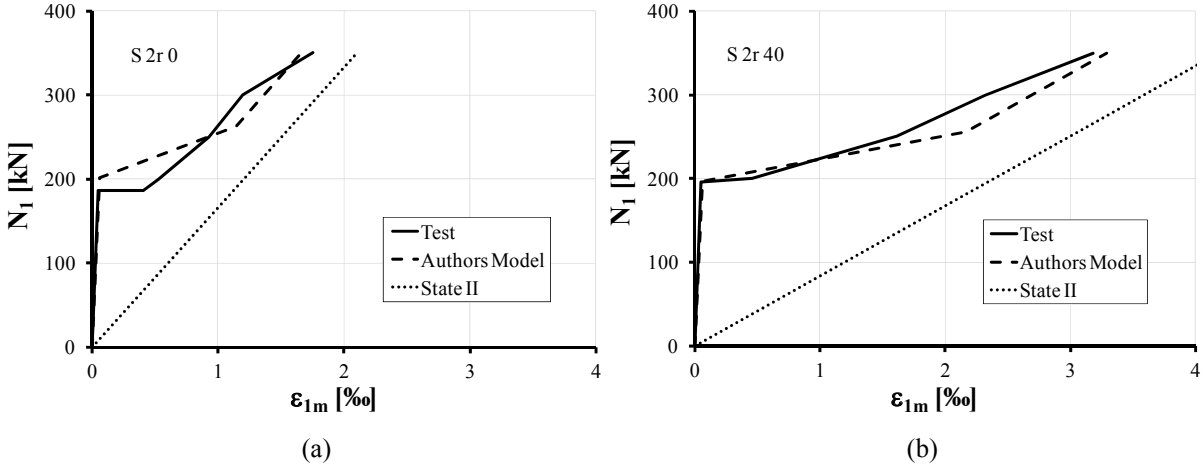

Figure 12: Comparison between authors model and test results (a) specimen S 2r 0 and (b) S 2r 40 from [9]

Own tests performed with biaxial loading show in Figure 13 a loading-deformation behaviour depending on the angle Θ and the interaction k =σ_2/σ_1. For Specimen Z1 with k = 1,0 and Θ = 0° the calculated values show only good accordance, when interaction of principal stresses has been considered. For Z3 the deformation behaviour is strongly influenced by biaxial tension with k = 0,5 and skew reinforcement with Θ = 45°. The calculated values from the proposed model agree very well with test results.

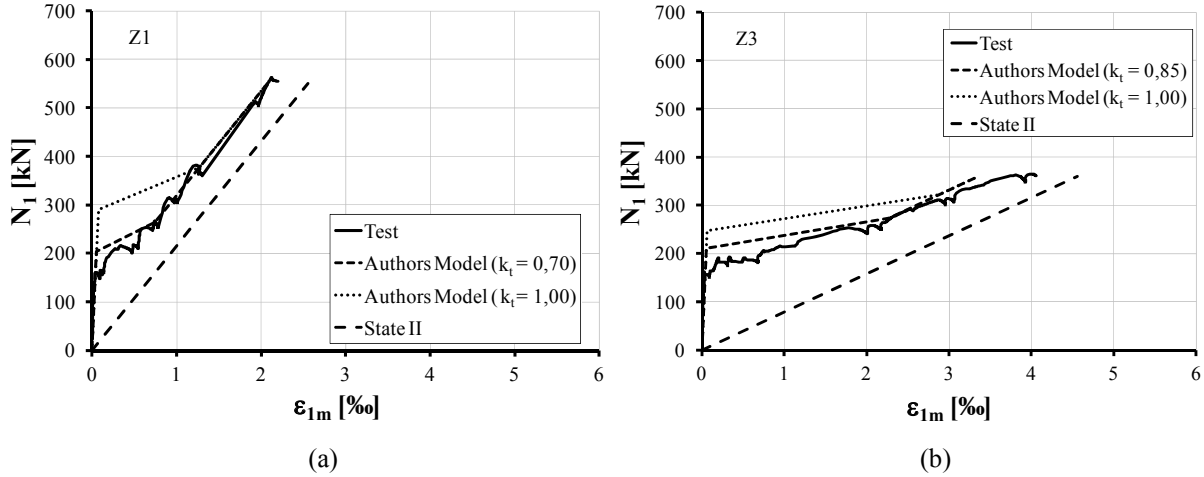

Figure 13: Comparison between authors model and own test results (a) specimen Z1 and (b) Z3

Uniaxial bending tests performed by Iványi & Lardi [9] have been compared to the proposed model as well for the elastic steel strains as for the ultimate loading (Figure 14). The prediction of the ultimate bending capacity for any kind of reinforcement orientation shows for all specimen good agreement with the test results (Table 2). Within calculations the inner lever arm has been supposed to be $z = 0{,}9 \cdot d$ and therefore $M_1 = N_1 \cdot z$. After first loading all specimen have been reloaded with cyclic steel stress (upper steel strains about 1 ‰) and 10^4 load cycles. In calculation for the first loading β_t has been supposed to be 0,4 and while cyclic loading $\beta_t = 0{,}25$. The increasing deformation due to cyclic loading has been considered through modification of the E-modulus of concrete depending on performed load cycles according to MC 2010 [3], see reference [11].

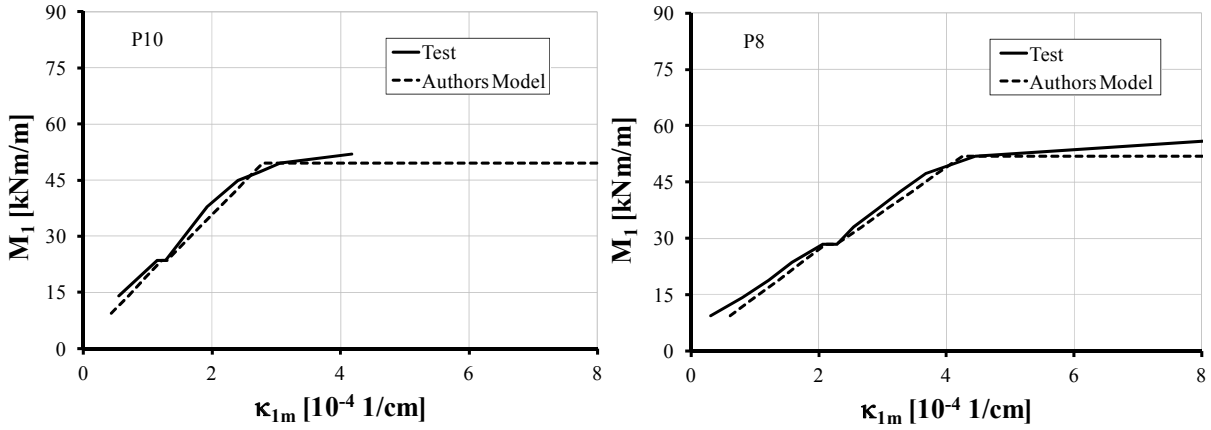

(a) (b)

Figure 14: Comparison between authors model and test results (a) specimen P10 and (b) P8 from [9]

Table 2: Load-carrying-capacity from tests of Iványi & Lardi [9] and authors model

No. [-]	Θ [°]	$f_{sy,x}$ [N/mm²]	$f_{sy,y}$ [N/mm²]	$f_{c,prism}$ [N/mm²]	$f_{ct,sp}$ [N/mm²]	$M_{1Rd,test}$ [kNm/m]	$M_{1Rd,cal}$ [kNm/m]	$M_{1Rd,test}$ / $M_{1Rd,cal}$ [-]
P5	60	429	501	20,8	2,2	16,9	16,1	1,05
P8	30	550	486	22,2	2,5	56,7	51,9	1,09
P10	0	525	495	29,0	2,2	51,9	49,6	1,05
P11	30	535	495	27,6	2,7	23,6	26,0	0,91
P12	30	540	538	31,5	2,5	42,5	33,1	1,28
P13	30	489	449	27,4	2,5	49,1	44,4	1,11
P15	30	469	469	27,0	2,3	80,3	73,7	1,09
							MW	1,08
							s	0,11
							v	0,10

The proposed model has been compared with values from combined in-plane loading tests performed by Vecchio & Collins [16]. The new model is able to predict the deformation behaviour for any in-plane action as well as the ultimate load carrying capacity (Figure 15). Beside good agreement in calculating the deformations with the new method, accordance of predicting the correct failure mode for every specimen has been achieved and documented in Table 3.

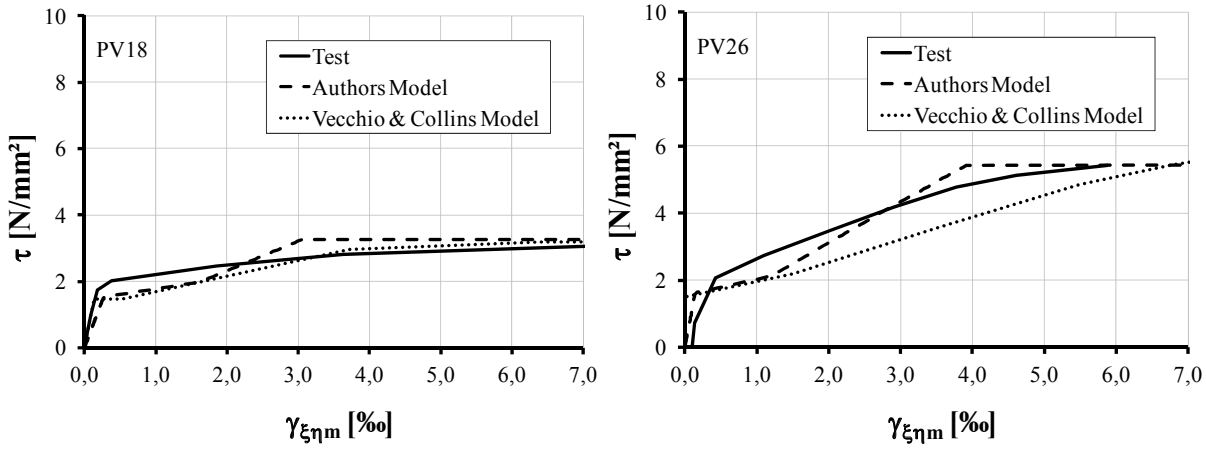

(a) (b)

Figure 15: Comparison between authors model and test results (a) specimen PV18 and (b) PV26 from [16]

Table 3: Load-carrying-capacity from tests of Vecchio & Collins [9] and authors model

								Authors Model			Vecchio & Collins Model	
No.	Θ	$f_{sy,x}$	$f_{sy,y}$	λ	$f_{c,cyl}$	f_{ct}	$\tau_{Rd,test}$	$\tau_{Rd,cal}$	$\tau_{Rd,test}$ / $\tau_{Rd,cal}$	failure	$\tau_{Rd,cal}$	$\tau_{Rd,test}$ / $\tau_{Rd,cal}$
[-]	[°]	[N/mm²]	[N/mm²]	[-]	[N/mm²]	[N/mm²]	[N/mm²]	[N/mm²]	[-]	[-]	[N/mm²]	[-]
PV2	45	428	428	1,0	23,5	1,7	1,16	1,20	0,97	S	1,61	0,72
PV3	45	662	662	1,0	26,6	1,9	3,07	3,19	0,96	S	3,20	0,96
PV4	45	242	242	1,0	26,6	1,9	2,89	2,57	1,12	S	2,59	1,12
PV6	45	226	226	1,0	29,8	2,0	4,55	4,65	0,98	S	4,76	0,96
PV10	45	276	276	1,8	14,5	1,2	3,97	3,86	1,03	S	3,68	1,08
PV11	45	235	235	1,4	15,6	1,3	3,56	3,56	1,00	S	3,59	0,99
PV12	45	469	269	4,0	16,0	1,3	3,13	3,07	1,02	S + R	2,94	1,06
PV13	45	248	-	∞	18,2	1,5	2,01	1,68	1,20	R	1,42	1,42
PV16	45	255	255	1,0	21,7	1,6	2,14	1,88	1,14	S	1,90	1,13
PV18	45	431	412	5,7	19,5	1,5	3,04	3,27	0,93	R	3,22	0,94
PV19	45	458	299	2,5	19,0	1,5	3,95	3,76	1,05	S + R	4,05	0,98
PV20	45	460	297	2,0	19,6	1,5	4,26	3,96	1,08	S	4,46	0,96
PV21	45	458	302	1,4	19,5	1,5	5,03	4,65	1,08	S	5,30	0,95
PV26	45	456	463	1,8	21,3	1,6	5,41	5,48	0,99	S	5,99	0,90

S = steel failure	MW	1,04	MW	1,01
R = crack plane failure	s	0,08	s	0,15
R + S = combined failure	v	0,07	v	0,15

f_{ct} from $f_{c,cyl}$ with k_s = 0,7 (loss of concrete tensile strength due to shrinkage)

7 CONCLUSIONS

Reinforced concrete is suitable to withstand the strong environment exposure in offshore structures. To fulfil the high requirements for the designing of these structures, adequate models are required. Today calculation methods show good accordance with experimental results, but have the disadvantage to be very extensive. The new approach has been developed in order to reduce the complex algorithms for shell structures to a possible limit and lead to highly accurate results. Its easy handling and programming are benefits of the new approach.

ACKNOWLEDGEMENT

The research work has been achieved with the financial support of the "German Research Foundation" (DFG) within the research project EM 203/3-1. All support is gratefully acknowledged.

REFERENCES

[1] Aoyagi, Y. “Analytical Approach to the Design of Orthogonally Reinforced Concrete Shell Elements to in-Plane Shear”, Proc. of JCI Colloq. on Shear Analysis of RC Structures, (1982).

[2] Aoyagi, Y. and Yamada, K. “An Experimental Approach to the Design of Network Reinforcement Against in-Plane Shear in Reinforced Concrete Containments”, 5th SMiRT Conference J4/7, (1979).

[3] CEB FIP “Model Code 2010”, First Complete Draft, Lausanne, (2010).

[4] CEB FIP “Concrete Structures for Oil and Gas Fields in Hostile Marine Environments”, State-of-the-Art Report (Bulletin 50), Task Group 1.5, Lausanne, (2009).

[5] EC 2: Design of Concrete Structures – Part 1-1: General Rules for Buildings, (2011).

[6] Empelmann, M. and Krakowski, W. “Crack Width Control of Construction Elements with Skew Reinforcement”, fib Symposium Prague, Long Edition, (2011).

[7] Empelmann, M. and Krakowski, W. “Experimentelle Untersuchungen zum Rissverhalten von Stahlbetonscheiben bei schiefwinkliger Bewehrung (Experimental Study to the Cracking Behaviour of Concrete Panels with Arbitrary Reinforcement Orientation, Paper in German)”, Festschrift Prof. M. Keuser, Universität der Bundeswehr München, (2012).

[8] FIP ”Recommendations for the Design of Concrete Sea Structures“, London, (1973).

[9] Iványi, G. and Lardi, R. “Trag- und Verformungsverhalten von netzbewehrten Stahlbetonplatten“, Forschungsberichte aus dem Fachbereich Bauwesen (No. 19). Universität Essen Gesamthochschule, (1982).

[10] Krakowski, W. and Henke, V. and Empelmann, M. “Rissbreitenberechnung bei schiefwinkliger Bewehrung (Abstract in English)”, Final Report: IRB T 3237, (2010).

[11] Krakowski, W. “Rissverhalten von Flächentragwerken aus Stahlbeton mit beliebig orientierter Bewehrung (Abstract in English)”, Submitted and Accepted Dissertation, Technische Universität Braunschweig, (2013).

[12] Mattock, A. “Shear Transfer in Concrete Having Reinforcement at an Angle to the Shear Plane”, ACI SP 42-2, 17–42, (1974).

[13] Peter, J. “Zur Bewehrung von Scheiben und Schalen für Hauptspannungen schiefwinklig zur Bewehrungsrichtung“, Dissertation, TH Stuttgart, (1964).

[14] Reddy, D. and Arockiasamy, M. “Offshore Structures”, Volume 1 & 2, Krieger Publishing Company, (1991).

[15] Vecchio, F. and Collins, M, “The Modified Compression-Field Theory for Reinforced Concrete Elements Subjected to Shear”, ACI Journal, 219–231, (1986).

[16] Vecchio, F. and Collins, M. “The Response of Reinforced Concrete to in-Plane Shear and Normal Stresses“, Publication No. 82-03, University of Toronto, (1982).

[17] Walraven, J. “Aggregate Interlock; A Theoretical and Experimental Analysis”. Dissertation. Delft University, (1980).